*Desalination and Water Treatment*
www.deswater.com
doi: 10.1080/19443994.2015.1004117

57 (2016) 5654–5672
March

Taylor & Francis
Taylor & Francis Group

# Nanomagnetite-loaded poly (acrylamide-co-itaconic acid) hydrogel as adsorbent for effective removal of $Mn^{2+}$ from contaminated water

Neeraj Sharma, Alka Tiwari*

*Department of Chemistry, Govt. V.Y.T. PG. Autonomous College, Durg (Chhattisgarh) 491001, India, Tel. +09098190861; email: neeraj.sharma.shyam@gmail.com (N. Sharma), Tel. +07415514000; Fax: +0788 2324783; emails: brnsbarc18@gmail.com, alkatiwari18@yahoo.co.in (A. Tiwari)*

Received 23 November 2014; Accepted 30 December 2014

ABSTRACT

The present research focuses on the adsorptive efficiency of nanomagnetite-loaded poly (acrylamide-co-itaconic acid) hydrogel for manganese removal from aqueous and contaminated solution by batch as well as column adsorption technique. The influence of pH, contact time, adsorbent dose, temperature, metal ion concentration, bed depth, feed flow rate and inlet metal ion concentration on the sensitivity of the removal process was inspected. The copolymer was synthesized and magnetized *in situ*. The sorption data was analyzed and fitted to linearized adsorption isotherm of the Langmuir and Freundlich equations, respectively. Equilibrium data fitted very well to the Freundlich model. The kinetics of sorption was analyzed using pseudo-first-order and pseudo-second-order kinetic models. Kinetic parameters, rate constants, equilibrium sorption capacities, and related correlation coefficients for each kinetic model were calculated. Different thermodynamic parameters i.e. $\Delta G^0$, $\Delta H^0$, and $\Delta S^0$ were also evaluated which proved the sorption to be feasible, spontaneous, and exothermic in nature. This hydrogel has been found to be an efficient adsorbent for manganese removal from water (>99% removal) and could be regenerated efficiently for further experiments.

*Keywords:* Nanomagnetite particles; Hydrogel; Isotherms; Kinetics; Thermodynamics

## 1. Introduction

Manganese reaches into water bodies due to disposal of untreated discharge from industries as well as leaching process of rocks. Numerous industrial activities, namely mining and metallurgical processes, manufacturing of dry cell batteries, ceramics, electrical coils, pigments, and paints, are the principle sources of manganese pollution into surface and ground water [1–4]. Burning of coal and oil also contributes to manganese pollution [5]. Manganese is present mainly in its divalent form ($Mn^{2+}$) in ground and surface water. Ground water containing high percentage of iron or manganese or both, shows lack of dissolved oxygen and high $CO_2$ content [6]. High manganese concentrations in drinking water can result in deposition of oxide in pipeline, water and laundry discoloration, and unpleasant metallic taste [7,8].

According to WHO, the level of contamination of manganese in drinking water should not exceed beyond 0.05 mg $dm^{-3}$ [6,9,10]. Water containing elevated concentrations of manganese is found to be toxic to humans and other living resources as well as

*Corresponding author.

reduces the quality of drinking water [11,12]. The toxicity of manganese occurs in the tissues of living organisms because of its bioaccumulation and non-biodegradable nature [13–17]. It acts as a pollutant due to its organoleptic properties [18]. Increased concentration of manganese in human beings affects the brain by depositing in basal ganglia which results in several neurological disorders [19].

Different techniques used for the removal of toxic metal ions from contaminated wastewater are filtration [20], chemical precipitation [21], chemical coagulation [22], flocculation [23], reverse osmosis [24], solvent extraction [25], membrane separation [26–28], ion exchange [29], and adsorption. The efficiency of most of these methods was found to be less due to less removal of heavy metals at very low concentrations, high operational cost, and contamination of recipient environment by their secondary effluent impact [30–33]. Presently, "Adsorption" is a widely accepted and very effective method for the removal of toxic metal ions from contaminated water [34]. Mondal [35], Mohan [36], Nassar [2], Guzel et al. [37], Okoniewska et al. [19], Rajic et al. [38] and Robinson-lora and Brennan [39] studied the adsorption of manganese ions using granular activated carbon (41%), lignite (25.84%), palm fruit bunch and maize cobs (79–50%), black carrot, impregnated activated carbon, natural zeolite tuff and chitin or chitin plus proteins, respectively.

In the present study, nanomagnetite-loaded poly (acrylamide-co-itaconic acid) hydrogel was characterized and applied as an efficient and effective adsorbent to remove Mn(II) from synthetic as well as contaminated water. The sorption of Mn(II) ions onto nanomagnetite-loaded PAI hydrogel was studied by applying batch as well as column equilibrium techniques. The efficiency of Mn(II) ions removal by magnetic PAI hydrogel was studied as a function of various factors i.e. pH, contact time, adsorbent dose, temperature, and initial metal ion concentration in batch system and different bed depth, feed flow rate, and inlet Mn(II) concentration in a fixed-bed column system.

For the purpose of comparison of adsorption capacity of PAI hydrogel with and without nanomagnetite impregnation, the adsorption experiments were conducted. The PAI hydrogel loaded with nanomagnetite showed very high removal of Mn(II) ions (99.50%) whereas the adsorbent without nanomagnetite gave only 80.45% removal. Hence, impregnation of nanomagnetite particles improved the efficiency of the novel adsorbent in the removal of Mn(II) ions from aqueous solution. In the copolymer of acrylamide and Itaconic acid, nanomagnetite particles were impregnated by *in situ* method because these nanoparticles have a tendency to aggregate, which reduces their high surface area to volume ratio and thus reduces the effectiveness of the nanomagnetite particles. Copolymer contains different functional groups which are involved in adsorption of Mn(II) ions and thus involve in removal of toxic Mn(II) ions from contaminated samples.

## 2. Materials and methods

### 2.1. Materials

The monomers acrylamide and itaconic acid were purchased from Loba Chemi, Mumbai and Himedia, Mumbai, India, respectively. N,N´-methylene-bis-acrylamide (cross-linker), potassium per sulfate (initiator), anhydrous ferric chloride, and ferrous chloride tetra hydrate were purchased from Molychem, Mumbai, India. Triple distilled, water was used throughout the experiments.

### 2.2. Synthesis of nanomagnetite-loaded PAI hydrogel

To a mixture of acrylamide and itaconic acid in 1:1 ratio, the cross linker (N,N´-methylene-bis-acrylamide) and initiator (potassium per sulfate) were added and heated at 70˚C in an electric oven for 1 h. The copolymeric hydrogel so formed was washed with distilled water and cut into small pieces. For *in situ* magnetization, these pieces were equilibrated in an aqueous solution of ferrous chloride (0.1 M) and ferric chloride (0.3 M) in 1:2 ratios for 24 h. The $Fe^{3+}/Fe^{2+}$ loaded pieces of copolymer were then added into ammonia solution and kept overnight. The magnetic hydrogel was then washed thoroughly with distilled water, dried, and crushed into a fine powder.

### 2.3. Swelling studies

The swelling characteristics were measured by immersing weighed sample of dry hydrogel in triple distilled water. The excess surface water in the swollen gel was removed by blotting and then the swollen gel was weighed. The swollen gel was blotted several times till three consecutive weights were obtained same within limits of experimental error of 1%.

#### 2.3.1. Determination of swelling ratio

The swelling ratio (SR) most commonly described as degree of swelling ($D_s$) is expressed as increase in weight/gm of dried hydrogel after keeping in contact with water for selected periods of time. The values of were calculated by Eq. (1).

$$\text{Swelling ratio (SR)} = \frac{W_s - W_d}{W_d} \quad (1)$$

where $W_s$ is the weight of swollen gel (g) at a given time and $W_d$ is the weight of dry gel (g).

#### 2.3.2. Determination of equilibrium degree of swelling

The equilibrium degree of swelling (EDS) was determined by immersing dry gel in triple distilled water at room temperature for a period of 72 h.

$$\text{EDS} = \frac{W_{eq} - W_d}{W_d} \quad (2)$$

where $W_{eq}$ is the weight of completely (equilibrium) swollen state of gel (g) and $W_d$ is the weight of dry gel (g). The value of EDS is given in Table 1.

#### 2.3.3. Determination of equilibrium water content

The equilibrium water content (EWC) is expressed in % on the weight of swollen gel at equilibrium, using Eq. (3).

$$\text{EWC} = \frac{W_{eq} - W_d}{W_{eq}} \times 100 \quad (3)$$

where, $W_{eq}$ is the weight of swollen gel at equilibrium and $W_d$ is the weight of the dry gel. The value of EWC is given in Table 1.

### 2.4. Characterization of magnetic copolymer

The adsorbent—"Nanomagnetite-loaded PAI Hydrogel" was characterized by XRD, AFM, SEM, and Fourier Transform Infrared Spectroscopy (FTIR) analysis.

Table 1
Swelling parameters of nanomagnetite-loaded PAI hydrogel

| S. No. | Parameters | Values |
|---|---|---|
| 1. | Equilibrium degree of swelling (EDS) (g $g^{-1}$) | 6.5 |
| 2. | Equilibrium water content (EWC) (%) | 86.67 |
| 3. | Theoretical equilibrium swelling $(S_{eq})_{max}$ (g $g^{-1}$) | 6.76 |
| 4. | Initial swelling rate ($r$) | 0.7449 |
| 5. | Swelling rate constant ($k_s$) | 0.0163 |

#### 2.4.1. XRD analysis

The crystalline nature of the bare nanomagnetite-loaded PAI hydrogel was studied on a Bruker D8 advanced X-ray Diffractometer with scanning range of 20–80° ($2\theta$) using Cu Kα radiation with wavelength of 1.5406Å (UGC- DAE, Indore, India).

#### 2.4.2. AFM analysis

The morphology and diameter of nanomagnetite particles was examined by contact mode AFM (NS-E, Digital Instrument INC, USA) using silicon nitrate tip. The sample was prepared for AFM analysis by placing a few drops of the suspension of $Fe_3O_4$ in 50% HCl on a cleaved mica sheet (UGC-DAE, Indore, India).

#### 2.4.3. SEM Analysis

To examine the morphological characteristics of nanomagnetite-loaded PAI hydrogel before and after Mn(II) adsorption, samples were viewed using a scanning electron microscope (SAIF, Punjab University, Chandigarh).

#### 2.4.4. FTIR analysis

FTIR spectra of unabsorbed (bare) and Mn(II) loaded adsorbent was recorded using Varian Vertex FTIR Spectrometer (UGC-DAE, Indore, India).

### 2.5. Preparation of stock solution

Stock solution of Mn(II) of 1,000 mg $dm^{-3}$ was prepared by dissolving 0.308 g $MnSO_4{\cdot}H_2O$ (AR) in 100 ml triple distilled water. Suitable concentrations of Mn(II) for batch and column experiments were prepared by diluting the stock solution with triple distilled water.

### 2.6. Sampling

Sampling was performed as per the standard procedures and techniques to ensure representation of contaminated water samples and industrial effluent. Effluent sample was collected from drains coming out of the industrial site. In order to avoid the surface impurities, surface water samples were collected from about 40–50 cm below the surface. For sampling of contaminated water, polythene bottles were rinsed with 0.1 N $HNO_3$, and then washed twice with triple distilled water. In order to analyze the metal ions, samples were filtered and acidified with conc. $HNO_3$ to

pH 2 and refrigerated at 4°C. For testing other parameters, virgin polythene cans were used for sample collection and analysis of samples was done within 48 h. Temperature, pH, and color of the samples were measured immediately after collection of samples at the sampling site by using thermometer, handy pH meter and by visual observations, respectively.

### 2.7. Sample preparation

Digestion of contaminated water samples were carried out by standard APHA methods which is necessary to destroy the organic contaminants, removal of ions that can interfere in analysis because heavy metal ions have a tendency to form complexes with organic contaminants present in water samples. For digestion purpose, 50 ml of sample was heated with 10 ml conc. $HNO_3$ in fume cupboard. During heating, $HNO_3$ was added in small portions until the clear and light colored solution was obtained. The heating was continued till the volume was reduced to 10 ml, then allowed to cool and volume was made to 50 ml with distilled water in standard flask and used for analysis.

### 2.8. Analytical techniques

The concentration of Mn(II) ions was determined using atomic absorption spectrometer (Varian AA-24-OFS model). Each experiment was carried out in triplicate under identical conditions to get the mean values.

### 2.9. Batch adsorption experiment

The adsorption experiments were carried out by batch method by varying pH, contact time, adsorbent dose, adsorbate concentration, and temperature. For adsorption experiments, nanomagnetite-loaded PAI hydrogel in the powdered form (0.1 g) and 20 ml $MnSO_4{\cdot}H_2O$ solution of 4 mg $dm^{-3}$ concentration at pH 6 and room temperature (25°C) was stirred for 1 h which was found to be sufficient time to attain equilibrium sorption. The amount of manganese ions present in solution (before and after adsorption) was determined by atomic absorption spectrometer.

The sorption degree (percentage removal) and sorption capacity of the sorbent was calculated by the following equations:

$$\text{Sorption degree} = \frac{(C_0 - C_e)}{C_0} \times 100\% \quad (4)$$

$$\text{Sorption capacity} = \frac{(C_0 - C_e) \cdot V}{m} \quad (5)$$

where $C_0$ and $C_e$ (mg $L^{-1}$) are the initial and equilibrium concentrations of manganese ions, respectively, $V_{sol}$ (L) is the volume of the manganese solution subjected to sorption, and $m_{sorb}$ (g) is the weight of sorbent.

### 2.10. Desorption experiment

Desorption studies indicate the nature of adsorption and recovery of valuable metals from wastewater and the sorbent. After the sorption experiments, the sorbent was collected by filtration, washed with distilled water, and was desorbed using 25 ml of $HNO_3$ of various strengths ranging from 0.02 to 0.2 M as an eluant. Desorption efficiency was calculated by using the following equation:

$$\text{Desorption efficiency} = \frac{\text{amount of Mn(II) desorbed}}{\text{amount of Mn(II) sorbed}} \times 100 \quad (6)$$

### 2.11. Kinetic study

The kinetic investigations were carried out to measure the adsorption rate under various experimental conditions such as pH, temperature, and equilibrium time. For the kinetic study, 0.1 g of adsorbent was shaken with 20 ml of manganese solution of desired concentrations and pH using a temperature-controlled shaker on a constant agitation speed at different time intervals and the adsorbed amount of manganese (II) ions was calculated same as adsorption equilibrium experiments.

### 2.12. Column experiment set up

Fixed-bed adsorption experiments were performed in a column made of polyethylene having an inner diameter of 0.5 cm and a height of 10 cm, at a constant temperature of 25°C. The column was packed with different bed heights of nanomagnetite-loaded PAI hydrogel on a glass-wool support. The experiments were performed at pH 6. The batch experimental results showed that the adsorption rate was high at pH 6. A known concentration of manganese solution was allowed to pass through the bed at a constant flow rate (1 ml $min^{-1}$) in a down-flow manner. For maintaining the constant flow rate of adsorbate solution, the peristaltic pump was used. The manganese solution was then collected at different time intervals until the column reached exhaustion and the concentration of Mn(II) ions was determined by atomic absorption spectrometer. The important design parameters such as column bed height, flow rate of metal solution into column, and initial concentration of metal solution have been investigated.

### 2.13. Analysis of column data

The efficiency of the column was evaluated by determining breakthrough curves. The time for breakthrough appearance and the shape of the breakthrough curve are very important characteristics for determining the operation and the dynamic response of an adsorption column. The breakthrough curves show the loading behavior of Mn(II) to be removed from solution in a fixed-bed and is usually expressed in terms of adsorbed metal concentration ($C_{ad}$ = inlet metal concentration ($C_0$)—outlet metal concentration ($C_t$)) or normalized concentration defined as the ratio of effluent metal concentration to inlet metal concentration ($C_t/C_0$) as a function of time or volume of effluent for a given bed height [40]. The breakthrough volumes $V_B$ and exhaustion volumes $V_E$ are the effluent volume at breakthrough time and exhaustion time, respectively. Effluent volume ($V_{eff}$) can be calculated from Eq. (7):

$$V_{eff} = Qt_{total} \tag{7}$$

where $t_{total}$ and $Q$ are the total flow time (min) and volumetric flow rate (ml $min^{-1}$). The area under the breakthrough curve (A) obtained by integrating the adsorbed concentration ($C_{ad}$; mg $dm^{-3}$) vs. $t$ (min) plot can be used to find the total adsorbed metal quantity (maximum column capacity). Total adsorbed metal quantity ($q_{total}$; mg $g^{-1}$) in the column for a given feed concentration and flow rate ($Q$) is calculated from Eq. (8):

$$q_{total} = \frac{Q \cdot (C_0 - C_t) \cdot t_{total}}{1,000} \tag{8}$$

Total amount of metal ion sent to column ($m_{total}$) is calculated from Eq. (9):

$$m_{total} = \frac{C_0 \cdot Q \cdot t_{total}}{1,000} \tag{9}$$

Total removal percent of Mn(II) is the ratio of the maximum capacity of the column ($q_{total}$) to the total amount of Mn(II) sent to column ($m_{total}$) from Eq. (10):

$$\text{Total removal } (\%) = \frac{q_{total}}{m_{total}} \times 100 \tag{10}$$

Equilibrium metal uptake ($q_{eq}$) (or maximum capacity of the column) in the column is defined by Eq. (11) as the total amount of metal sorbed ($q_{total}$) per g of sorbent (X) at the end of the total flow time:

$$q_{eq} = \frac{q_{total}}{X} \tag{11}$$

### 2.14. Column desorption study

Column desorption study was carried out after the column adsorption studies were conducted, at 25 ± 0.2°C, by using 0.1 M $HNO_3$ solution at flow rate of 1 ml $min^{-1}$ and 1 cm bed depth to provide sufficient exchangeable $H^+$ ions for 330 min and then washed with hot distilled water and could be reused for further adsorption experiment.

## 3. Results and discussion

### 3.1. Swelling studies

Dynamic swelling of nanomagnetite-loaded PAI hydrogel at different absorbing time in water was measured at room temperature. Results of these experiments indicated that the increase in weight of the swollen hydrogels is directly related to the duration of swelling. The swelling behavior observed could be associated with the absorption mechanism, which, in turn, is determined by the diffusion process. The swelling rate is slow during the first few minutes; it indicates that the initial swelling is due primarily to the water penetrating into the polymeric gel through capillary and diffusion. Then the penetrated water is absorbed by hydrophilic groups such as itaconic acid and acrylamide through formation of hydrogen bonds. The

swelling is driven by repulsion of hydrophilic groups inside the network and osmotic pressure difference between the gels and the external solution. The swelling rate is fast during the first 60 min and gradually slows down until the equilibrium swelling is reached. It was evident that the SR increases sharply upon prolongation of swelling time up to 180 min then levels off.

### 3.2. Kinetics of swelling

The swelling kinetics of the prepared hydrogel was undertaken with view of clarifying the controlling mechanism of the swelling processes. A simple kinetic analysis represented by a second-order equation was applied in this study using the following relationship [41].

$$\frac{\mathrm{dSR}}{\mathrm{d}t} = k_s(S_{eq} - S)^2 \tag{12}$$

where $k_s$ is the swelling rate constant and $S_{eq}$ is the degree of swelling at the state of equilibrium. After integration, when the initial conditions $S = 0$ at $t = 0$ and $S = \mathrm{S}$ at $t = \mathrm{t}$ are applicable, Eq. (12) is modified as follows:

$$\frac{t}{\mathrm{SR}} = A + Bt \tag{13}$$

in which

$$B = \frac{1}{S_{eq}} \tag{14}$$

is the inverse of the maximum or equilibrium swelling;

$$A = \frac{1}{k_s S_{eq^2}} \tag{15}$$

is the reciprocal of the initial swelling rate of the hydrogel and $k_s$ is the swelling rate constant. The initial swelling rate ($r$), the swelling rate constant ($k_s$), and the values of theoretical equilibrium swelling ($S_{eq}$)max of hydrogel were calculated from the slope and the intersection of the lines. The results are presented in Table 1.

### 3.3. Characterization of nanomagnetite-loaded PAI hydrogel

The nanomagnetite-loaded PAI hydrogel was synthesized and characterized by the following instrumental methods.

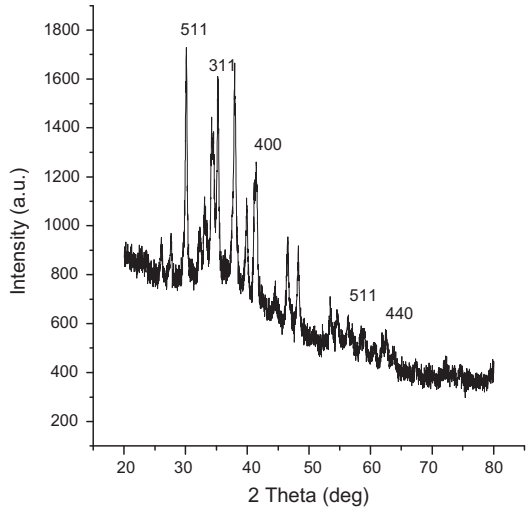


Fig. 1. XRD pattern of nanomagnetite-loaded PAI hydrogel.

#### 3.3.1. XRD analysis

The XRD pattern for the nanomagnetite-loaded PAI hydrogel is shown in Fig. 1. Five characteristic peaks ($2\theta = 30.09$, 35.44, 43.07, 56.96, and 62.55), marked by their indices [(5 1 1), (3 1 1), (4 0 0), (5 1 1), and (4 4 0)], were observed for nanomagnetite-loaded PAI hydrogel. The position and relative intensities of all diffraction peaks in Fig. 1 match well with those from the JCPDS file No. 89-5984 for magnetite ($Fe_3O_4$) and reveal that the prominent phase formed is $Fe_3O_4$ and the resultant nanoparticles of super paramagnetic iron oxide were pure magnetic with cubic structure. Magnetite is obtained according to the reaction:

$$2FeCl_3 + FeCl_2 + 8NH_4OH \rightarrow Fe_3O_4 + 8NH_4Cl + 4H_2O$$

#### 3.3.2. AFM analysis

The morphology of the nanomagnetite particles, using contact mode AFM, was found to be spherical, having size distribution in two different diameter (height) ranges of 10–20 nm (mean height: 15 nm) and 40–110 nm (mean height: 50 and 80 nm) as shown in Fig. 2. However, some larger particle size in figure may be a result of agglomeration of smaller magnetite nanoparticles in order to reduce the inherent large surface energies for magnetite nanoparticles.

#### 3.3.3. SEM analysis

The SEM image of the sorbent surface is shown in Fig. 3 which clearly indicates the incorporation of

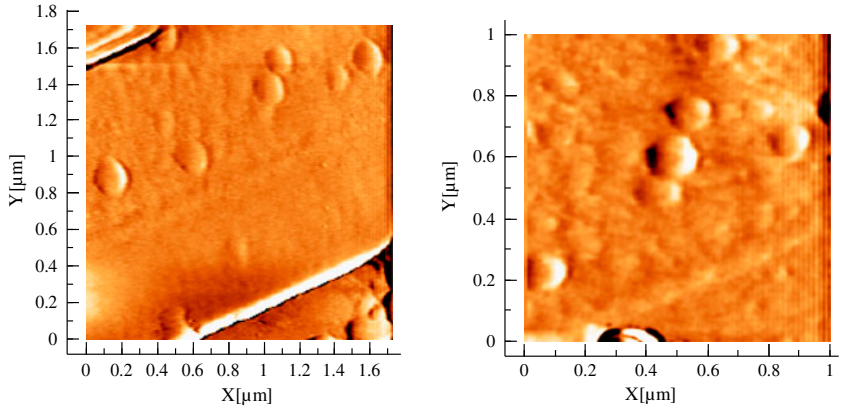


Fig. 2. AFM topographic images of magnetic nanoparticles on mica.

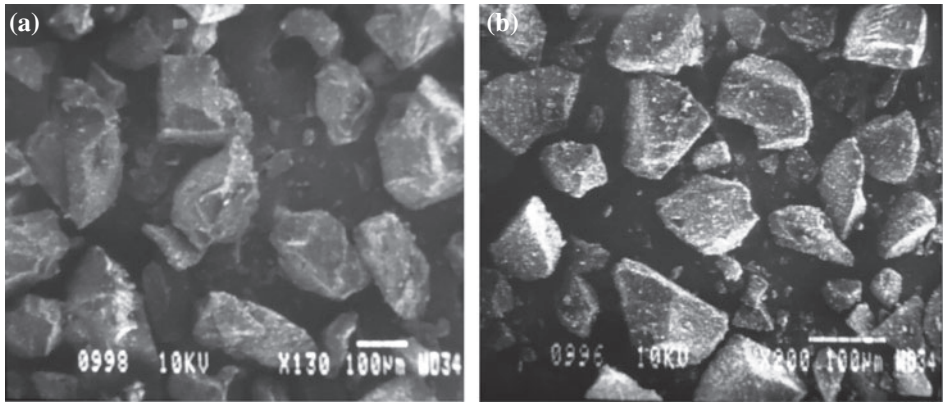


Fig. 3. SEM images of bare (a) nanomagnetite-loaded PAI hydrogel, (b) nanomagnetite-loaded PAI hydrogel after Mn(II) adsorption.

nanomagnetite within copolymeric matrix. The surface appears quite heterogeneous and uneven. The presence of large voids make the surface quit heterogeneous and porous, which justify significant adsorption capacity of sorbent.

### 3.3.4. FTIR analysis

FTIR of bare and manganese adsorbed nanomagnetite-loaded PAI hydrogel are shown in Fig. 4(a) and (b), respectively. The simultaneous presence of band in the regions 3,616–3,372 $cm^{-1}$ is due to $OH^-$ stretching of hydroxyl groups of carboxylic (–COOH) group. $CH_2$ (methylene group) stretching is obtained at 2,214.55 $cm^{-1}$. The FTIR analysis indicated the band due to acrylamide at 3,398 $cm^{-1}$, 1,659.18 $cm^{-1}$, 1,604 $cm^{-1}$, and 1,395.93 $cm^{-1}$ attributed to N–H stretching, C=O stretching, N–H bending, and C–N stretching, respectively, which are

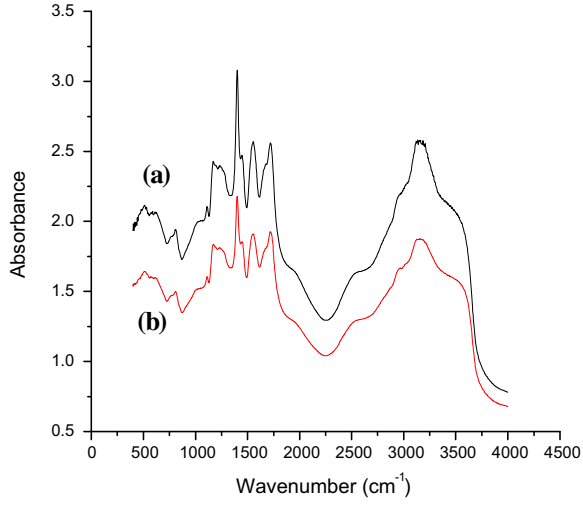


Fig. 4. FTIR pattern of (a) nanomagnetite-loaded PAI hydrogel before sorption of Mn(II) ions, (b) nanomagnetite-loaded PAI hydrogel after sorption of Mn(II) ions.

the characteristics of the amide ($CONH_2$) group. Absorption peaks due to itaconic acid were also observed at 1,725.86 $cm^{-1}$, 1,558.96 $cm^{-1}$ for C=O and C–O stretching of the carboxylic (–COOH) group, respectively. The characteristic peak at 524.14 $cm^{-1}$ relates to Fe–O group, which indicates the loading of nano iron oxide particles on PAI hydrogel because the surface of iron-oxide with negative charges has an affinity towards PAI hydrogel, the magnetite nanoparticles could be loaded into protonated copolymer by the electrostatic interaction and chemical reaction through N,N´-methylene -bis-acrylamide cross linking. In Fig. 4(b), a slight change in shape and intensity of absorbance (due to $–CONH_2$ and –COOH groups) has been noticed, which indicate that electron rich nitrogen of amide group of acrylamide moiety and $–COO^-$ group of itaconic acid moiety involve in removal of iron. Change in the peak position and intensity for Fe–O group stretching from 568 to 489 $cm^{-1}$ indicate that iron coordinate with electron-rich oxygen of magnetite nanoparticles ($Fe_3O_4$).

### 3.4. Adsorption isotherms

In order to describe in which manner manganese ion concentration will interact with nanomagnetite-loaded PAI hydrogel surface and are useful to find out the efficiency of adsorbent for manganese removal, adsorption isotherms were studied. To interpret the probable mechanism of sorption, equilibrium sorption isotherms serve as the most important data. In this study, Langmuir and Freundlich models were applied to evaluate experimental result.

#### 3.4.1. Langmuir isotherm

To depict adsorption phenomenon, Langmuir isotherm is employed, which is based on the assumption that through monolayer sorption, adsorbate uptake occurs on a homogenous surface without interact with adsorbed molecules [42]. The isotherm follows the typical Langmuir adsorption pattern as shown in Fig. 5.

Applicability of the data to the Langmuir adsorption isotherm was tested and it was noticed that the data were not fitted well into the linearized Langmuir adsorption isotherm which is given by Eq. (16).

$$\frac{C_e}{q_e} = b\frac{1}{Q_0} + \frac{C_e}{Q_0} \tag{16}$$

where $q_e$ is the amount of solute adsorbed per unit weight of adsorbent (mg $g^{-1}$), $C_e$ is the equilibrium concentration of solute in the bulk solution (mg $dm^{-3}$),

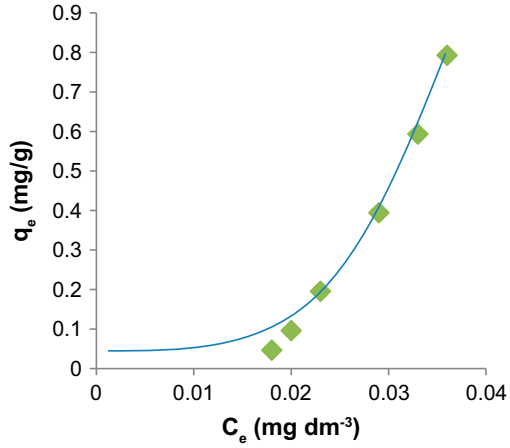


Fig. 5. Adsorption isotherm of nanomagnetite-loaded PAI hydrogel for manganese.

$Q_0$ is the monolayer adsorption capacity (mg $g^{-1}$) and $b$ is a constant related to the free energy of adsorption. The values of constant $Q_0$ and $b$ are given in Table 2. From Table 2, the value of correlation coefficient ($R^2 = 0.725$) for Mn(II) ions is very low, indicating a poor fit of monolayer Langmuir isotherm to the sorption of Mn(II) by nanomagnetite-loaded PAI hydrogel.

#### 3.4.2. Freundlich isotherm

The Freundlich isotherm, an empirical expression, is based on the fact of heterogeneity of adsorbent surface and multilayer adsorption of adsorbate molecule onto binding sites situated on the sorbent surface [43]. The linear form of the Freundlich model can be shown by Eq. (17).

$$\log q_e = \log K_f + \frac{1}{n}\log C_e \tag{17}$$

where the intercept, log $K_f$, is a measure of adsorbent capacity and the slope $1/n$ is the sorption intensity. The values of constant $K_f$ and $n$ are given in Table 2. The value of correlation coefficient ($R^2 = 0.977$) shows a good fit of the experimental data with the Freundlich

Table 2
Constants of Langmuir and Freundlich isotherm models for Mn(II) ions

| Langmuir constant | | | Freundlich constant | | |
|---|---|---|---|---|---|
| $Q_0$ | $b$ | $R^2$ | $K_f$ | $n$ | $R^2$ |
| −0.065 | −0.036 | 0.725 | 0.601 | 0.257 | 0.977 |

model. The value of n was between 0 and 10, suggesting relatively strong sorption of manganese ions onto the surface of nanomagnetite-loaded PAI hydrogel. So it is reasonable to predict that sorptive behavior of manganese on nanomagnetite-loaded PAI hydrogel may take place in multilayer on the adsorbent surface.

### 3.5. Adsorption kinetic modeling

In order to explain the sorption process, it is necessary to deal with adsorption kinetics because it provides information about rate at which the process occurs as well as factors affecting the sorption rate. The progress of adsorption process was observed at different time intervals (0–120 min), which clearly indicates that the sorption of manganese ions increases with the increase in time and then levels off after 60 min.

#### 3.5.1. First-order reversible model

The sorption of manganese from liquid phase to solid may be considered as a reversible reaction with an equilibrium state being established between two phases. A simple first-order reaction model was, therefore, used to correlate the rates of reaction, which can be expressed by Eq. (18).

$$\ln\ [1 - U_{(t)}] = -k''t \tag{18}$$

where $k''$ is the overall rate constant and calculated by following equation:

$$K'' = k_1 + \left(1 + \frac{1}{K_c}\right) = k_1 + k_2 \tag{19}$$

where $k_1$, $k_2$, and $K_c$ are the forward rate constant, backward rate constant, and equilibrium constant, respectively, and can be obtained from the following equation.

$$K_c = \frac{k_1}{k_2} = \frac{C_{Ae}}{C_e} \tag{20}$$

$$U_{(t)} = \frac{X}{X_e} \tag{21}$$

where $U_{(t)}$ is called the fractional attainment of equilibrium. Therefore, a plot of $-\ln[1 - U_{(t)}]$ vs. time (min) will give a straight line. The overall rate constant $k''$ for a given concentration of manganese was calculated by considering the slope of the straight line and by using Equations 19 and 20, the equilibrium constant $K_c$, forward and backward rate constants $k_1$ and $k_2$ were calculated and shown in Table 3. From Table 3, it can be seen that the forward rate constant for the removal of manganese is much higher than the backward rate constant, namely the desorption process. The uptake of manganese by magnetic adsorbent was reversible and thus has good potential for the removals/recovery of manganese from aqueous solutions.

#### 3.5.2. Second-order kinetic model

The second-order kinetic scheme was proposed as follows.

$$\frac{1}{C} = k_2 \frac{t}{C_0} + \frac{1}{C_0} \tag{22}$$

where $C$ and $C_0$ being the concentrations of metal ions in solution at any time $t$ and zero time (i.e. initial concentration), respectively, and $k_2$ is the rate constant for adsorption. The value of $k_2$ is given in Table 4.

In order to inspect the controlling mechanism of sorption phenomena such as mass transfer and chemical reaction, the pseudo-first-order and pseudo-second-order kinetic models were used to evaluate the kinetic profile of manganese adsorption onto nanomagnetite-loaded PAI hydrogel. These models depend on two criteria; (1) the value of regression coefficient should be acceptably high ($R^2$) and (2) the calculated $q_e$ value should be near to the experimental $q_e$ value.

Table 3
The first order reversible reaction rate constant for the removal of Mn(II) ions by nanomagnetite-loaded PAI hydrogel

| Manganese (mg dm$^{-3}$) | Overall rate constant $k'' = k_1 + k_2$ (min$^{-1}$) | Equilibrium constant $K_c$ | Forward rate constant $k_1$ (min$^{-1}$) | Backward rate constant $k_2$ (min$^{-1}$) | Correlation coefficient $R^2$ |
|---|---|---|---|---|---|
| 4 | 0.041 | 99 | 0.0406 | 0.0004 | 0.979 |

Table 4
The second-order reaction rate constant for the removal of Mn(II) ions by nanomagnetite-loaded PAI hydrogel

| Initial manganese concentration (mg dm$^{-3}$) | Second-order rate equation | | Intraparticle rate constant |
|---|---|---|---|
| | $k_2$ | $R^2$ | $k_p$ (mg$^{-1}$ min$^{-1/2}$) |
| 4 | 0.1466 | 0.999 | 0.011 |

### 3.5.3. Pseudo-first-order kinetic model

The expression of pseudo-first-order kinetic model (Lagergren equation) is given by Eq. (23).

$$\log\ (q_e - q_t) = \log\ q_e - \frac{k_{ad}}{2.303} t \tag{23}$$

where $q_t$ and $q_e$ are the adsorption capacity (mg g$^{-1}$) at time $t$ and at equilibrium, respectively. $k_{ad}$ is the pseudo-first-order rate constant of the adsorption. The assumption behind this model is that the sorption rate is proportional to the number of vacant sites available and the process taking place exclusively onto single site per ion [44,45]. By using linear plot of log ($q_e - q_t$) vs. $t$, the values of regression coefficient ($R^2$) and $k_{ad}$ for manganese sorption at concentration 4 mg dm$^{-3}$ were calculated and are listed in Table 5. It was observed from the results that the kinetics of Mn(II) ion sorption onto nanomagnetite-loaded PAI hydrogel did not fit this model as the value of regression coefficient was relatively low and a large difference was observed between calculated and experimental $q_e$ value.

### 3.5.4. Pseudo-second-order kinetic model

The expression of pseudo-second-order kinetic model is given by Eq. (24).

$$\frac{t}{q_t} = \frac{1}{(k_2' q_t^2)} + \frac{1}{q_e} t \tag{24}$$

where $k_2' q_t^2 = h$ (mg g$^{-1}$ min$^{-1}$) can be regarded as the initial adsorption rate when $t \to 0$ and $k_2'$ (g mg$^{-1}$ min$^{-1}$) is the rate constant of the pseudo-second-order equation. The assumption behind this kinetic model is that the rate of sorption is controlled by chemisorption mechanism which involves sharing or transfer of electron between the adsorbent and adsorbate [46]. By using linear plot of $t/q_t$ vs. $t$, the values of regression coefficient ($R^2$) and $k_2'$ and h can be determined from the slope and intercept of the plot, respectively. It was noted that the kinetics of Mn (II) ion sorption onto nanomagnetite-loaded PAI hydrogel could be fitted to this model as extremely high value of correlation coefficient ($R^2$) as well as a great agreement between the calculated and experimental $q_e$ values were obtained as shown in Table 5.

### 3.5.5. Intra particle diffusion

Besides adsorption at the outer surface, there is also possibility of intraparticle diffusion from the outer surface into the pores of adsorbent material. The adsorption mechanism of a sorbate onto the adsorbent follows three steps viz. film diffusion, pore diffusion, and intraparticle transport [47]. Though there is a high possibility for pore diffusion to be the rate-limiting step in a batch process, the adsorption rate parameter which controls the batch process for most of the contact time is the intraparticle diffusion. Thus, in order to evaluate the rate controlling step, a plot was drawn between the amounts of manganese adsorbed on magnetic copolymer $q_t$ vs. $t^{1/2}$. The rate constant for intraparticle diffusion is obtained using the Eq. (25).

$$q_t = k_p t^{1/2} \tag{25}$$

where $k_p$ is the intra particle diffusion rate constant (mg$^{-1}$ min$^{-1/2}$). The value of $k_p$ determined from the slope of the linear portion of the curve, which is given in Table 4.

Table 5
Comparison between the estimated adsorption rate constants, $q_e$ and correlation coefficients associated with the pseudo-first-order and the pseudo-second-order rate equations

| Initial manganese concentration (mg dm$^{-3}$) | Pseudo-first-order rate equation | | | Pseudo-second-order rate equation | | | | |
|---|---|---|---|---|---|---|---|---|
| | $k_{ad}$ (min$^{-1}$) | $q_e$ cal (mg g$^{-1}$) | $R^2$ | $k_2'$ (g mg$^{-1}$ min$^{-1}$) | $q_e$ cal (mg g$^{-1}$) | $R^2$ | $h$ (mg g$^{-1}$ min$^{-1}$) | $q_e$ exp (mg g$^{-1}$) |
| 4 | 2.0220 | 0.9616 | 0.979 | 1.3184 | 0.7994 | 1 | 0.8425 | 0.7920 |

### 3.6. Thermodynamic study

By applying Eq. (26), different thermodynamic parameters like free energy ($\Delta G^0$), enthalpy ($\Delta H^0$), and entropy ($\Delta S^0$) change of sorption can be evaluated.

$$K_c = \frac{C_{Ae}}{C_e} \tag{26}$$

where $K_c$ is the equilibrium constant, $C_e$ is the equilibrium concentration of metal ion in solution (mg dm$^{-3}$), and $C_{Ae}$ is the solid-phase concentration at equilibrium (mg dm$^{-3}$). In order to determine the $\Delta G^0$, $\Delta H^0$, and $\Delta S^0$ values, The $K_c$ values were used.

$$\Delta G^0 = -\mathrm{RT}\,2.303 \log K_c \tag{27}$$

where $\Delta G^0$ is the free energy of sorption (kJ mol$^{-1}$), $T$ is the absolute temperature (Kelvin), and $R$ is the universal gas constant (8.314 J mol$^{-1}$ K).

The $K_c$ may be expressed in terms of the $\Delta H^0$ (kJ mol$^{-1}$) and $\Delta S^0$ (J mol$^{-1}$ K) as a function of temperature.

$$\log\ K_c = \frac{\Delta S^0}{2.303R} - \frac{\Delta H^0}{2.303\mathrm{RT}} \tag{28}$$

According to Eq. (28), from the slope and the intercept of the linear plot of log $K_c$ vs. $1/T$ the values of $\Delta H^0$ and $\Delta S^0$ were determined, as shown in Table 6. The $\Delta G^0$ values at different temperatures were computed with the help of Eq. (27). It was observed that with the increase in temperature from 298 to 328 K, sorption of manganese onto adsorbent decreases, as shown in Fig. 9, indicating exothermic nature of the process. In this study, the values of $\Delta H^0$ and $\Delta S^0$ were found to be −74.616 kJ mol$^{-1}$ and −0.214 J mol$^{-1}$ K, respectively, for 4 mg dm$^{-3}$ manganese concentration. The negative values of $\Delta G^0$ indicate the feasibility and spontaneous nature of sorption process. The negative value of $\Delta H^0$ shows the exothermic nature of sorption and the negative value of $\Delta S^0$ indicates an increment in the randomness at solid-solution interface during manganese ion fixation on active sites of nanomagnetite-loaded PAI hydrogel.

It has been reported that electrostatic interaction occurs between metal ions and adsorption sites of adsorbent (physisorption) if $\Delta G^0$ values up to −20 kJ mol$^{-1}$ and sharing or transfer of electron between the adsorbent and adsorbate occurs (chemisorptions) when $\Delta G^0$ values more negative than −40 kJ mol$^{-1}$. In this work, the values obtained for $\Delta G^0$ were < −12 kJ mol$^{-1}$ indicating physisorption is the predominant mechanism during sorption of manganese [48].

### 3.7. Factors affecting adsorption

#### 3.7.1. Effect of pH

In sorption process, pH plays an important role as it affects the active sites of the adsorbent surface as well as the chemistry of metal in water [49,50]. To determine the effect of pH on the manganese sorption process onto nanomagnetite-loaded PAI hydrogel the pH of the solution varies from 2 to 8. It was observed that with the increase in pH from 2 to 6, the percentage removal of manganese was also increased while decrease in percentage removal was noticed after pH 6, as shown in Fig. 6. So pH 6 was selected as optimum pH for sorption process. $H^+$ ions compete with manganese ions for binding sites on adsorbent surface at low pH by hindering manganese ions to reach the active sites of adsorbent. At pH higher than 8, $OH^-$ ions interact with manganese ions to form manganese hydroxide; thus, manganese ions get precipitated.

#### 3.7.2. Effect of contact time

The effect of sorption time using 0.1 g of nanomagnetite-loaded PAI hydrogel and 20 ml of 4 mg dm$^{-3}$ solution of Mn(II) ions is shown in Fig. 7. It was observed that the sorption of manganese increased with increasing contact time and become almost constant after 60 min. The percent manganese removal is higher at the beginning; this is probably due to

Table 6
Thermodynamic parameters for the adsorption of Mn(II) ions onto nanomagnetite-loaded PAI hydrogel

| Initial manganese concentration (mg dm$^{-3}$) | $\Delta H^0$ (kJ mol$^{-1}$) | $\Delta S^0$ (J mol$^{-1}$ K) | $\Delta G^0$ (kJ mol$^{-1}$) | | | |
|---|---|---|---|---|---|---|
| | | | 25 °C | 35 °C | 40 °C | 50 °C |
| 4 | −74.616 | −0.214 | −11.49 | −8.02 | −5.85 | −5.08 |

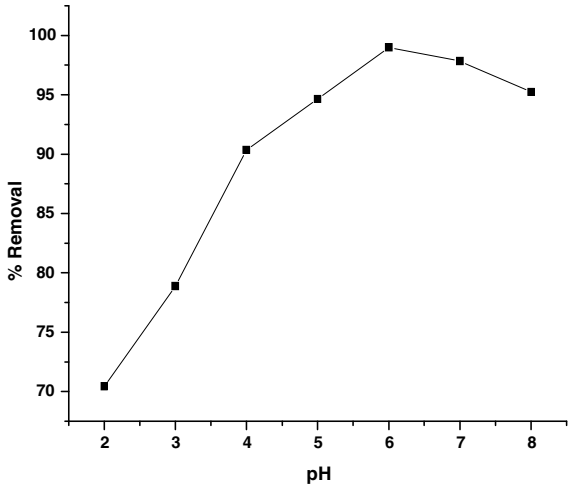


Fig. 6. Effect of time variation on manganese removal through nanomagnetite-loaded PAI hydrogel = 0.1 g, pH 6, temp. = 25 ± 0.2˚C.

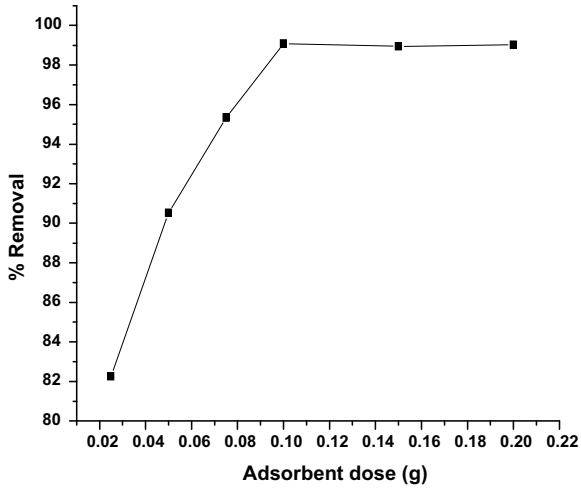


Fig. 8. Effect of adsorbent dose variation on manganese removal through nanomagnetite-loaded PAI hydrogel pH 6, time = 60 min, temp. = 25 ± 0.2˚C.

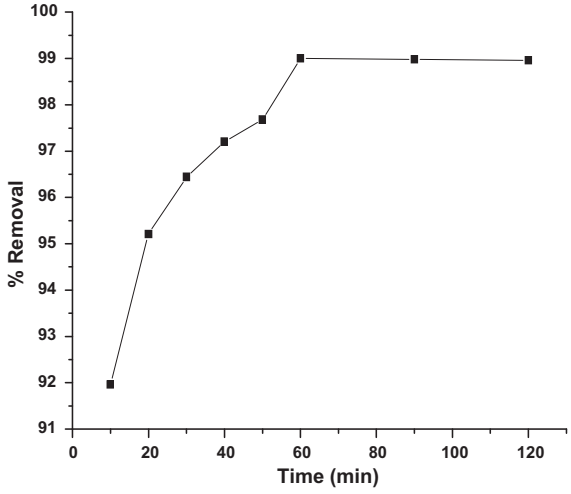


Fig. 7. Effect of pH variation on manganese removal through nanomagnetite-loaded PAI hydrogel = 0.1 g, time = 60 min, temp. = 25 ± 0.2˚C.

availability of larger surface area at beginning for manganese sorption. The equilibrium was attained in 1 h; hence, sorption time of 1 h was used as optimum time in further experiments.

### 3.7.3. Effect of adsorbent dosage

The effect of the adsorbent dose on the sorption of manganese ions from the aqueous solution was inspected by varying the sorbent amounts from 0.025 to 0.2 g using a fixed manganese concentration (4 mg $dm^{-3}$) at room temperature (25˚C). Fig. 8 shows that with an increase in the amount of adsorbent, the percentage removal of manganese ions increases rapidly as at higher adsorbent dose, large surface area is greatly available. When the adsorbent dose was increased from 0.025 to 0.2 g, a considerable increase in manganese uptake was observed. Beyond this, further addition of the sorbent did not cause any remarkable change in the sorption. The maximum removal of manganese was obtained at the adsorbent dose of 0.1 g.

### 3.7.4. Effect of temperature

In the removal process of metal ions from aqueous solutions, temperature plays a significant role. In order to optimize the effect of temperature on the removal of manganese by nanomagnetite-loaded PAI hydrogel, the temperature varied from 25 to 55˚C. The maximum uptake of manganese ions was obtained at 25˚C. It can be seen from Fig. 9 that the percentage removal of Mn(II) ions decreased from 99.04 to 86.55% as the temperature increases from 25 to 55˚C. This is due to the fact that the binding forces that hold manganese ions with active sites on the copolymer become weakened mainly because of decreased surface activity, suggesting that exothermic process is involved in sorption of manganese ions onto adsorbent.

### 3.7.5. Effect of initial concentration of Mn(II) ions

The metal uptake mechanism is particularly dependent on the heavy metal concentration. The effect of

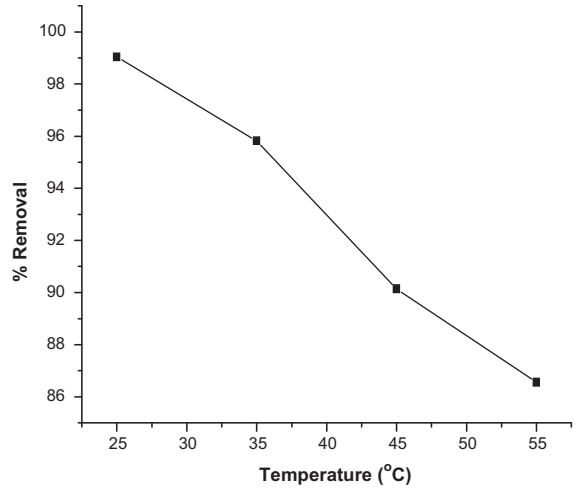


Fig. 9. Effect of temperature variation on mangnese removal through nanomagnetite-loaded PAI hydrogel = 0.1 g, pH 6, time = 60 min.

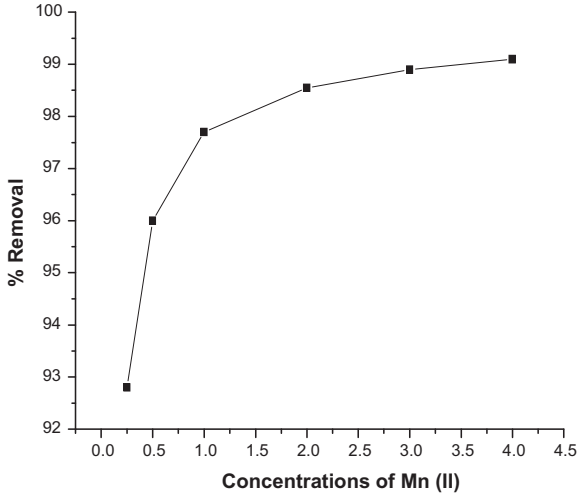


Fig. 10. Effect of different concentration on manganese removal through nanomagnetite-loaded PAI hydrogel = 0.1 g, pH 6, time = 60 min, temperature = 25 ± 0.2°C.

initial concentration of manganese ions onto percent manganese removal was studied in the range of 0.25–4 mg $dm^{-3}$ as shown in Fig. 10. It was noticed that the percent of manganese removal increased with the increase of manganese concentration. The inspected increase is quite obvious, as a large number of metal ions arrive at interface on increasing the solute concentration and thus get adsorbed.

### 3.8. Batch desorption studies

Desorption results indicated that 78.92, 84.18, 90.54, 98.22, 99.98, and 999.95% of Mn(II) were removed from the surface of the sorbent containing 0.7920 mg $g^{-1}$ of Mn(II) using 0.02, 0.04, 0.06, 0.08, 0.1, and 0.2 M $HNO_3$ strength, respectively, at 25°C temperature. Complete desorption of manganese (II) ions from the sorbent nearly took place by 0.1 M $HNO_3$ solution. The polymer showed almost the same metal ion adsorption capacity after repeated regeneration. It may be stated that in the acid medium, protons compete with manganese ions and displace the maximum amount of adsorbed manganese. Hence, ion exchange mechanism is important in connection with adsorption–desorption process for adsorbent.

### 3.9. Column studies of adsorption of Mn(II) ions onto nanomagnetite-loaded PAI hydrogel

Several operational factors such as bed depth ($Z$), flow rate ($Q$), and initial adsorbate concentration ($C_0$) affect the shape of a breakthrough curve and maximum capacity of the column. In this study, the effect of these parameters on breakthrough curve and maximum capacity of the column was investigated.

#### 3.9.1. Effect of bed depth

Accumulation of metal ions in the fixed bed column largely depends on the quantity of sorbent added in the column. The breakthrough curve for Mn(II) adsorption for three different bed depths (0.25, 0.5, and 1 cm) at constant adsorbate feed flow rate (1 ml $min^{-1}$) and adsorbate inlet concentration (4 mg $dm^{-3}$) is shown in Fig. 11. It was noticed that both the breakthrough time and exhaustion time showed an increase with increasing bed depth. A higher uptake was observed at higher bed height due

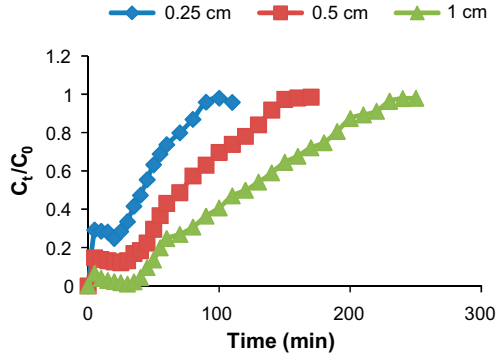


Fig. 11. The effect of bed depth on breakthrough curve at temperature = 25 ± 0.2°C, pH 6, bed depth of nanomagnetite-loaded PAI hydrogel = 0.25, 0.5 and 1 cm, flow rate = 1 ml $min^{-1}$ and Mn(II) initial concentration = 4 mg $dm^{-1}$.

Table 7
The effect of bed depth on breakthrough curve at temperature = 25 ± 0.2°C, pH 6, bed depth of nanomagnetite-loaded PAI hydrogel = 0.25, 0.5 and 1 cm and flow rate = 1 ml $min^{-1}$ and Mn(II) initial concentration = 4 mg $dm^{-3}$

| Bed depth (cm) | Flow rate (ml $min^{-1}$) | Inlet manganese ion concentration (mg $dm^{-3}$) | $t_{total}$ (min) | $m_{total}$ (mg) | $q_{total}$ (mg) | $q_{eq}$ (mg $g^{-1}$) | Removal (%) |
|---|---|---|---|---|---|---|---|
| 0.25 | 1 | 4 | 110 | 0.440 | 0.331 | 3.310 | 75.22 |
| 0.5 | 1 | 4 | 170 | 0.680 | 0.598 | 2.990 | 87.94 |
| 1 | 1 | 4 | 250 | 1.000 | 0.990 | 2.476 | 99 |

to the increase in the specific surface area of the adsorbent, which provides more fixation of the Mn(II) ions with more binding sites for the adsorption process to proceed. These results are also in agreement with those referred to the literature [51–54]. The increase in bed depth would increase the mass transfer zone. The mass transfer zone in a column moves from entrance of the bed and proceeds towards the exit. Hence, for the same influent concentration and fixed flow rate, an increase in bed depth would create a longer distance for the mass transfer zone to reach the exit, subsequently resulting in an extended breakthrough time. For higher bed depth, the increase of adsorbent mass would provide a larger service area leading to an increase in the volume of treated solution [55]. Also, an increase in the maximum bed adsorption capacity ($q_0$) was noticed at the breakthrough point with the increase in bed depth. The values are given in Table 7.

### 3.9.2. Effect of flow rate

The effect of feed flow rate on the adsorption of Mn(II) ions on nanomagnetite-loaded PAI hydrogel was investigated by varying the feed flow rate (1, 2, and 3 ml $min^{-1}$) at a constant adsorbent bed depth of 1 cm and inlet adsorbate concentration of 4 mg $dm^{-3}$, as shown by the breakthrough curve in Fig. 12. The trend of the curves showed that at higher flow rate, the front of the adsorption zone quickly reached the top of the column. This implies that the column was saturated early. Lower flow rate resulted in longer contact time, as well as a shallow adsorption zone.

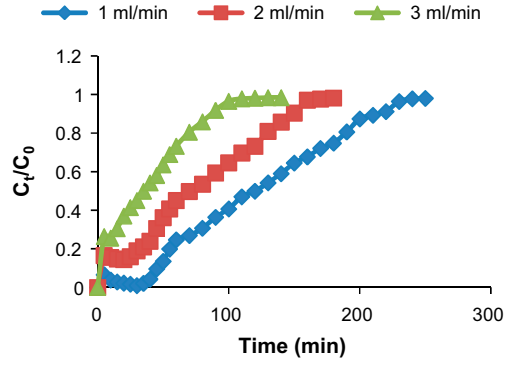


Fig. 12. The effect of flow rate on breakthrough curve at Temperature = 25 ± 0.2°C, pH 6, flow rate = 1, 2 and 3 ml $min^{-1}$, bed height = 1 cm and Mn(II) initial concentration = 4 mg $dm^{-3}$.

Higher flow rates are seen by the steeper curve with relatively early breakthrough and exhaustion time; they resulted in less adsorption uptake [56]. Also at higher flow rate, the rate of mass transfer increased, thus the amount of Mn(II) adsorbed onto the unit bed height (mass transfer zone) increased as reported elsewhere [57]. The values are given in Table 8.

### 3.9.3. Effect of initial manganese ion concentrations

The effect of inlet manganese concentration on the column performance was studied by varying the inlet concentration of manganese between 2, 3, and 4 mg $dm^{-3}$, taking the same adsorbent bed depth (1 cm) and flow rate (1 ml $min^{-1}$). Fig. 13 illustrated

Table 8
Results of breakthrough curve at different flow rates for adsorption of Mn(II) ions onto nanomagnetite-loaded PAI hydrogel at temperature = 25 ± 0.2°C, pH 6

| Flow rate (ml $min^{-1}$) | Bed depth (cm) | Inlet manganese ion concentration (mg $dm^{-3}$) | $t_{total}$ (min) | $m_{total}$ (mg) | $q_{total}$ (mg) | $q_{eq}$ (mg $g^{-1}$) | Removal (%) |
|---|---|---|---|---|---|---|---|
| 1 | 1 | 4 | 250 | 1.000 | 0.990 | 2.476 | 99 |
| 2 | 1 | 4 | 180 | 1.440 | 1.233 | 3.083 | 85.62 |
| 3 | 1 | 4 | 140 | 1.680 | 1.250 | 3.125 | 74.40 |

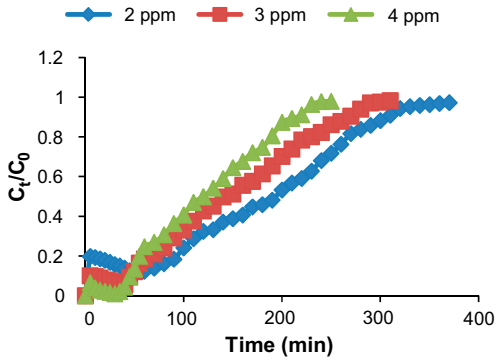


Fig. 13. The effect of inlet adsorbate concentration on breakthrough curve at temperature = 25 ± 0.2℃, pH 6, initial Mn(II) ion concentration = 2, 3 and 4 mg $dm^{-3}$, bed depth = 1 cm and flow rate = 1 ml $min^{-1}$.

breakthrough curves, which show that the columns exhausted faster at higher adsorbate inlet concentration (4 mg $dm^{-3}$), hence gave a steeper curve showing an earlier breakthrough point. Similar trends have also been reported elsewhere [56,58]. With the increase in adsorbate inlet concentration, the breakthrough time ($t_b$) was found to decrease because of quick saturation of the column. An extended breakthrough curve was obtained by the decrease in inlet concentration, suggesting a higher volume of solution to be treated. This may be explained by the fact that a lower concentration gradient may cause a slower transport which will result in diffusion coefficient or mass transfer coefficient [59]. The values are given in Table 9.

### 3.10. Column desorption studies

Desorption results indicated 99.50% recovery of Mn(II) ions from the surface of the sorbent using 0.1 M $HNO_3$ in 330 min at 25℃ temperature. The nanomagnetite-loaded PAI hydrogel showed almost the same metal ion adsorption capacity after the repeated regeneration. It may be stated that, in acidic medium, protons compete with Mn(II) ions and displace the maximum amount of adsorbed manganese. Hence, ion exchange mechanism is important in connection with adsorption–desorption process for adsorbent.

### 3.11. Mechanism of uptake

The nanomagnetite-loaded PAI hydrogel contains carboxyl and amide groups as confirmed by FTIR analysis, and are responsible for binding the toxic Mn (II) ions on the surface. The proposed mechanism of binding the Mn(II) ions on various sites available at adsorbent surface (Fig. 14) may be explained as follows.

(1) Carboxylate groups ($–COO^-$) of itaconic acid moiety of copolymer interact with Mn(II) ions.
(2) Mn(II) ions co-ordinate with the electron-rich nitrogen of amide group of acrylamide moiety of copolymer.
(3) In addition, within the copolymer matrix, these Mn(II) ions may also co-ordinate with the electron rich oxygen of magnetite nanoparticles.

### 3.12. Application

The metal polishing industrial wastewater and contaminated surface and ground water samples were collected and the optimized conditions as set in Batch as well as Column techniques for maximum removal of toxic metal ions were applied, to get the pure water for drinking and other purposes.

#### 3.12.1. Removal process

(1) For batch adsorption study, 20 ml sample water was shaken with 0.1 g of nanomagnetite-loaded PAI hydrogel for 60 min at 6 pH and room temperature (25℃). The amount of manganese present in sample (before and

Table 9
Results of breakthrough curve at different inlet adsorbate concentration for adsorption of Mn(II) ions onto nanomagnetite-loaded PAI hydrogel at temperature = 25 ± 0.2℃, pH 6

| Inlet manganese ion concentration (mg $dm^{-3}$) | Bed depth (cm) | Flow rate (ml $min^{-1}$) | $t_{total}$ (min) | $m_{total}$ (mg) | $q_{total}$ (mg) | $q_{eq}$ (mg $g^{-1}$) | Removal (%) |
|---|---|---|---|---|---|---|---|
| 2 | 1 | 1 | 370 | 0.740 | 0.653 | 1.633 | 88.24 |
| 3 | 1 | 1 | 310 | 0.930 | 0.879 | 2.198 | 94.52 |
| 4 | 1 | 1 | 250 | 1.000 | 0.990 | 2.476 | 99 |

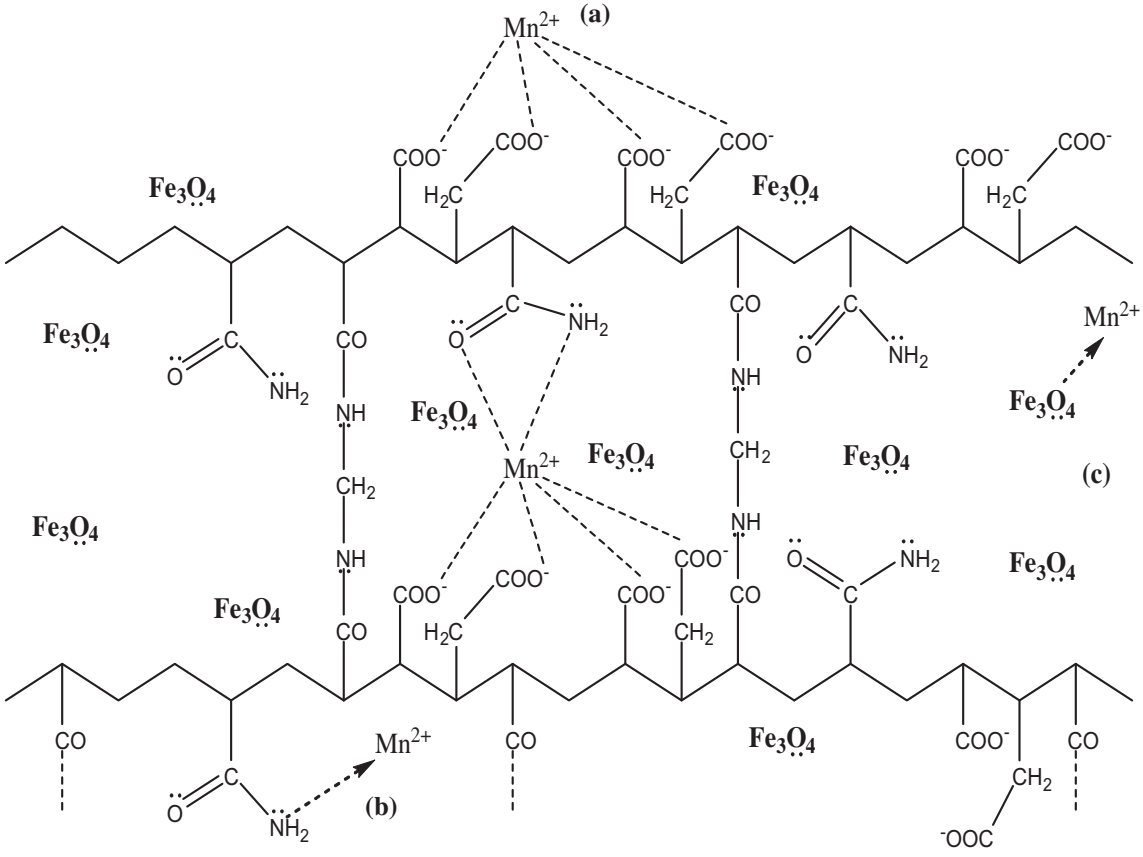


Fig. 14. Scheme of mechanism of Mn(II) ions uptake by nanomagnetite-loaded PAI hydrogel through: (a) Carboxylate groups of itaconic acid moiety, (b) electron rich nitrogen of amide group of acrylamide moiety, and (c) electron rich oxygen of magnetite nanoparticles.

Table 10
Application of nanomagnetite-loaded PAI hydrogel in the removal of manganese from metal polishing industrial effluent

| Name of adsorbents | Name of metal ions | Concentration of manganese in contaminated water (mg $dm^{-3}$) | % Removal in batch adsorption system | % Removal in column adsorption system |
|---|---|---|---|---|
| Nanomagnetite-loaded poly (acrylamide-co-itaconic acid) hydrogel | Manganese | 3.7918 | 99.04 | 99.55 |

after adsorption) was determined by atomic absorption spectrometer.

(2) For column adsorption study, contaminated water was allowed to pass through 1 cm column filled with nanomagnetite-loaded PAI hydrogel at 1 ml $min^{-1}$ feed flow rate. The manganese solution was then collected at different time intervals till the exhaustion of column and the concentration of Mn(II) ions was determined by atomic absorption spectrometer.

Table 10 shows the results of manganese removal from metal polishing industrial wastewater.

## 4. Conclusions

The nanomagnetite-loaded PAI hydrogel has been found to be an effective, efficient, and a cheap adsorbent for high removal of manganese from aqueous solution as well as contaminated water by batch and column method. The maximum percentage removal (99%) occurred at pH 6 and 25°C temperature in

60 min in batch method. The equilibrium sorption data fitted the Freundlich model better than Langmuir isotherm model. Thermodynamic parameters depicted the exothermic nature of adsorption and a favorable process for manganese removal. The pseudo-second-order reaction rate model described the kinetic data best for manganese sorption process. The effects of bed depth, inlet feed concentration, and flow rate on Mn(II) ion adsorption were investigated in column method and the experimental breakthrough curves were obtained. The experiments were performed at 1 ml $min^{-1}$ flow rate, 1 cm bed depth, and 4 mg $dm^{-3}$ inlet manganese ion concentration at pH 6. It was observed that equilibrium metal uptake ($q_0$) increased with increase in flow rate and inlet manganese ion concentration and decreased with increase in bed depth. Both breakthrough point and exhaustion time increased with increase in bed depth and inlet manganese ion concentration and decreased with increase in flow rate. The nanomagnetite-loaded PAI hydrogel could be repeatedly used in the adsorption studies by adsorption—desorption cycle without detectable losses in their initial adsorption capacities. The calculated column parameters could be scaled up for the design of fixed-bed columns for effective and efficient removal of toxic metal ions from water.

## Acknowledgments

The authors would like to express thanks to the Department of Atomic Energy, BRNS-BARC, Mumbai, India for providing financial assistance. Authors are also grateful to UGC-DAE Consortium for Scientific Research, Indore, India for FTIR analysis and AIIMS, New Delhi, India for TEM analysis.

## References

[1] J. Mejía-Saavedra, S. Sánchez-Armass, G.E. Santos-Medrano, R. González-Amaro, I. Razo-Soto, R. Rico-Martínez, F. Díaz-Barriga, Effect of coexposure to DDT and manganese on fish water invertebrates: Pore water from contaminated rivers and laboratory studies, Environ. Toxicol. Chem. 24 (2005) 2037–2044.

[2] M.M. Nassar, Adsorption of $Fe^{3+}$ and $Mn^{2+}$ from ground water onto maize cobs using batch adsorber and fixed bed column, Sep. Sci. Technol. 41 (2007) 251–258.

[3] P. Roccaro, C. Barone, G. Mancini, F.G.A. Vagliasindi, Removal of manganese from water supplies intended for human consumption: A case study, Desalination 210(1–3) (2007) 205–214.

[4] A. Omri, M. Benzina, Removal of manganese (II) ions from aqueous solutions by adsorption on activated carbon derived a new precursor: *Ziziphus spina christi* seeds, Alexandria Eng. J. 51(4) (2012) 343–350.

[5] K. Kannan, Fundamental of Environmental Pollution, S. Chand Co. Limited, New Delhi, 1995, p. 51.

[6] C.N. Sawyer, P.L. McCarty, G.F. Parkin, Chemistry for Environmental Engineering and Science, TaTa McGraw-Hill, New Delhi, 2003, p. 660.

[7] L.L. Sly, M.C. Hoodgkinson, V. Arunpariojana, Deposition of manganese in a drinking water distribution system, Appl. Environ. Microbiol. 56 (1990) 628–639.

[8] K.V. Heal, P.E. Kneale, A.T. Donald, Manganese mobilization and runoff process in upland catchments, in: British Hydrological Society, Presented at the 5th National Hydrology Symposium, Edinburgh, 1995, pp. 911–918.

[9] D.A. Kumar, Environmental Chemistry, New Age International, New Delhi, 2004, p. 280.

[10] A. Celik, A. Demirbaş, Removal of heavy metal ions from aqueous solutions via adsorption onto modified lignin from pulping wastes, Energy Sources 27 (2005) 1167–1177.

[11] C.L. Keen, S. Zidenberg-Cherr, Manganese in Health and Disease, CRC Press, London, 1994, p. 193.

[12] P. Nyberg, P. Andersson, E. Degerman, H. Borg, E. Olofsson, Labile inorganic manganese—An overlooked reason for fish mortality in acidified streams, Water Air Soil Pollut. 85 (1995) 333–340.

[13] G. Cimino, A. Passerini, G. Toscano, Removal of toxic cations and Cr(VI) from aqueous solution by hazelnut shell, Water Res. 34 (2000) 2955–2962.

[14] A. Kebede, T. Wondimu, Distribution of trace elements in muscle and organs of Tilapia, *Oreochromis niloticus* from Lakes Awassa and Ziway, Bull. Chem. Soc. Ethiop. 18 (2004) 119–130.

[15] E.J. Underwood, Trace Elements in Humans and Animal Nutritio, Academic Press, NewYork, NY, 1997, p. 42.

[16] W. Kaim, B. Schwedski, Bio-inorganic Chemistry, John Wiley and Sons, Chichester, 1994, p. 35.

[17] K.C. Pillalli, Heavy Metals in Aquatic Environment, Wiley Eastern Limited, New Delhi, 1985, p. 74.

[18] S.R. Taffarel, J. Rubio, On the removal of $Mn^{2+}$ ions by adsorption onto natural and activated Chilean zeolites, Miner. Eng. 22 (2009) 336–343.

[19] E. Okoniewska, J. Lach, M. Kacprzak, E. Neczaj, The removal of manganese, iron and ammonium nitrogen on impregnated activated carbon, Desalination 206 (2007) 251–258.

[20] H. Bessbousse, T. Rhlalou, J.F. Verchère, L. Lebrun, Removal of heavy metal ions from aqueous solutions by filtration with a novel complexing membrane containing poly(ethyleneimine) in a poly(vinyl alcohol) matrix, J. Membr. Sci. 307 (2008) 249–259.

[21] J.O. Esalah, M.E. Weber, J.H. Vera, Removal of lead from aqueous solutions by precipitation with sodium di-(n-octyl) phosphate, Sep. Purif. Technol. 18 (2000) 25–36.

[22] A.G. El Samrani, B.S. Lartiges, F. Villiéras, Chemical coagulation of combined sewer overflow: Heavy metal removal and treatment optimization, Water Res. 42 (2008) 951–960.

[23] E. Ofir, Y. Oren, A. Adin, Comparing pretreatment by iron of electro-flocculation and chemical flocculation, Desalination 204 (2007) 87–93.

[24] Y. Benito, M.L. Ruíz, Reverse osmosis applied to metal finishing wastewater, Desalination 142 (2002) 229–234.

[25] S.K Gupta, N.S. Rathore, J.V. Sonawane, A.K. Pabby, P. Janardan, R.D. Changrani, P.K. Dey, Dispersion-free solvent extraction of U(VI) in macro amount from nitric acid solutions using hollow fiber contactor, J. Membr. Sci., 300 (2007) 131–136.
[26] C.A. Cooper, Y.S. Lin, M. Gonzalez, Separation properties of surface modified silica supported liquid membranes for divalent metal removal/recovery, J. Membr. Sci. 229 (2004) 11–25.
[27] R.S. Juang, R.C. Shiau, Metal removal from aqueous solutions using chitosan-enhanced membrane filtration, J. Membr. Sci. 165 (2000) 159–167.
[28] M.M. Nasef, A.H. Yahaya, Adsorption of some heavy metal ions from aqueous solutions on Nafion 117 membrane, Desalination 249 (2009) 677–681.
[29] L.C. Lin, J.K. Li, R.S. Juang, Removal of Cu(II) and Ni (II) from aqueous solutions using batch and fixed-bed ion exchange processes, Desalination 225 (2008) 249–259.
[30] J. Müslehiddinoglu, U. Uludag, H.O. Ozbelege, Z. Yilmaz, Determination of heavy metal concentration in feed and permeate streams of polymer enhanced ultrafiltration process, Talanta 46 (1998) 1557–1565.
[31] K.J. Kim, V. Chen, A.G. Fane, Characterization of clean and fouled membranes using metal colloids, Membr. Sci. 88 (1994) 93–101.
[32] D.C. Sharma, C.F. Forster, A preliminary examination into the adsorption of hexavalent chromium using low cost adsorbents, Bioresour. Technol. 47 (1994) 257–264.
[33] C. Namasivayam, D. Sangeetha, Removal of chromium (VI) by $ZnCl_2$ activated coir pith carbon, Toxicol. Environ. Chem. 88 (2006) 219–233.
[34] S. Liang, X. Guo, N. Feng, Q. Tian, Isotherms, kinetics and thermodynamic studies of adsorption of $Cu^{2+}$ from aqueous solutions by $Mg^{2+}/K^{+}$ type orange peel adsorbents, J. Hazard. Mater. 174 (2010) 756–762.
[35] P. Mondal, C. Balomajumder, B. Mohanty, A laboratory study for the treatment of arsenic, iron, and manganese bearing ground water using $Fe^{3+}$ impregnated activated carbon: Effects of shaking time, pH and temperature, J. Hazard. Mater. 144 (2007) 420–426.
[36] D. Mohan, S. Chander, Single, binary and multicomponent sorption of iron and manganese on lignite, J. Colloid Interface Sci. 299 (2006) 76–87.
[37] F. Guzel, H. Yakut, G. Topal, Determination of kinetic and equilibrium parameters of the batch adsorption of Mn(II), Co (II), Ni (II) and Cu (II) from aqueous solution by black carrot (*Daucus carota L.*) residues, J. Hazard. Mater. 153 (2008) 1275–1287.
[38] N. Rajic, D. Stojakovic, S. Jevtic, N. Zabukovec Logar, J. Kovac, V. Kaucic, Removal of aqueous manganese using the natural zeolitic tuff from the *Vranjska banja* deposite in Serbia, J. Hazard. Mater. 172 (2009) 1450–1457.
[39] M.A. Robinson-Lora, R.A. Brennan, Biosorption of manganese onto chitin and associated proteins during the treatment of mine impacted water, Chem. Eng. J. 162 (2010) 565–572.
[40] Z. Aksu, F. Gönen, Biosorption of phenol by immobilized activated sludge in a continuous packed bed: prediction of breakthrough curves, Process Biochem. 39 (2004) 599–613.
[41] M.A. Enas, S.A. Fatima, Swelling kinetic study and characterization of crosslinked hydrogels containing silver nanoparticles, J. Appl. Polym. Sci. 117 (2010) 2168–2174.
[42] F.A. Dawodu, K.G. Akpomie, Simultaneous adsorption of Ni(II) and Mn(II) ions from aqueous solution unto a Nigerian kaolinite clay, J. Mater. Res. Technol. 3 (2014) 129–141.
[43] A. Witek-Krowiak, R.G. Szafran, S. Modelski, Biosorption of heavy metals from aqueous solutions onto peanut shell as a low-cost biosorbent, Desalination 265 (2011) 126–134.
[44] H. Lalhruaitluanga, K. Jayaram, M.N.V. Prasad, K.K. Kumar, Lead(II) adsorption from aqueous solutions by raw and activated charcoals of *Melocanna baccifera* Roxburgh (bamboo)—A comparative study, J. Hazard. Mater. 175 (2010) 311–318.
[45] D.H.K. Reddy, D.K.V. Ramana, K. Seshaiah, A.V.R. Reddy, Biosorption of Ni(II) from aqueous phase by *Moringa oleifera* bark, a low cost biosorbent, Desalination 268 (2011) 150–157.
[46] Y. Ding, D. Jing, H. Gong, L. Zhou, X. Yang, Biosorption of aquatic cadmium (II) by unmodified rice straw, Bioresour. Technol. 114 (2012) 20–25.
[47] T.S. Singh, K.K. Pant, Equilibrium, kinetics and thermodynamic studies for adsorption of As(III) on activated alumina, Sep. Purif. Technol. 36 (2004) 139–147.
[48] N.T. Abdal Ghani, G.A. Eichaghaby, Influence of operating conditions on the removal of Cu, Zn, Cd and Pb ions from wastewater by adsorption, Int. J. Environ. Sci. Technol. 4 (2007) 451–456.
[49] P. Waranusantigul, P. Pokethitiyook, M. Kruatrachue, E.S. Upatham, Kinetics of basic dye (methylene blue) biosorption by giant duckweed (*Spirodela polyrrhiza*), Environ. Pollut. 125 (2003) 385–392.
[50] H. Hasar, Adsorption of nickel(II) from aqueous solution onto activated carbon prepared from almond husk, J. Hazard. Mater. 97 (2003) 49–57.
[51] Z. Zulfadhly, M.D. Mashitah, S. Bhatia, Heavy metals removal in fixed-bed column by the macro fungus *Pycnoporus sanguineus*, Environ. Pollut. 112 (2001) 463–470.
[52] J.T. Nwabanne, P.K. Igbokwe, Adsorption performance of packed bed column for the removal of lead (II) using oil palm fibre, Int. J. Appl. Sci. Technol. 2 (2012) 106–115.
[53] E. Malkoc, Y. Nuhoglu, Removal of Ni(II) ions from aqueous solutions using waste of tea factory: Adsorption on a fixed-bed column, J. Hazard. Mater. 135 (2006) 328–336.
[54] E. Malkoc, Y. Nuhoglu, Fixed bed studies for the sorption of chromium(VI) onto tea factory waste, Chem. Eng. Sci. 61 (2006) 4363–4372.
[55] V. Sarin, T.S. Singh, K.K. Pant, Thermodynamic and breakthrough column studies for the selective sorption of chromium from industrial effluent on activated eucalyptus bark, Bioresour. Technol. 97 (2006) 1986–1993.
[56] V.C. Taty-Costodes, H. Fauduet, C. Porte, Y.S. Ho, Removal of lead (II) ions from synthetic and real effluents using immobilized *Pinus svlvestris* sawdust: Adsorption on a fixed column, J. Hazard. Mater. 123 (2005) 135–144.

[57] D.C.K. Ko, J.F. Porter, G. McKay, Optimised correlations for the fixed-bed adsorption of metal ions on bone char, Chem. Eng. Sci. 55 (2000) 5819–5829.
[58] K. Vijayaraghavan, J. Jegan, K. Palanivelu, M. Velan, Removal of nickel (II) ions from aqueous solution using crab shell particles in a packed bed up flow column, J. Hazard. Mater. 113 (2004) 223–230.
[59] K. Vijayaraghavan, J. Jegan, K. Palanivelu, M. Velan, Batch and column removal of copper from aqueous solution using brown marine alga *Turbinaria ornala*, Chem. Eng. J. 106 (2005) 177–184.